AMMRC TR 70-18

AD

AD 712307

MICROSTRUCTURAL AND FRACTOGRAPHIC STUDIES OF BORON CARBIDE SUBJECTED TO BALLISTIC IMPACT AND STATIC FLEXURAL LOADING

WILLIAM A. BRANTLEY
CERAMICS DIVISION

D D C
RECEIVED
OCT 9 1970
A

August 1970

This document has been approved for public release and sale; its distribution is unlimited.

ARMY MATERIALS AND MECHANICS RESEARCH CENTER
Watertown, Massachusetts 02172

CLEARINGHOUSE

The findings in this report are not to be construed as an official Department of the Army position, unless so designated by other authorized documents.

Mention of any trade names or manufacturers in this report shall not be construed as advertising nor as an official indorsement or approval of such products or companies by the United States Government.

DISPOSITION INSTRUCTIONS

Destroy this report when it is no longer needed.
Do not return it to the originator.

AMMRC TR 70-18

MICROSTRUCTURAL AND FRACTOGRAPHIC STUDIES OF BORON CARBIDE SUBJECTED TO BALLISTIC IMPACT AND STATIC FLEXURAL LOADING

Technical Report by

WILLIAM A. BRANTLEY, CPT, Ord C

August 1970

D/A Project 1T062105A330
AMCMS Code 502E.11.296
Ceramics Materials Research for Army Materiel
Agency Accession Number DA OB4802

This document has been approved for public release and sale; its distribution is unlimited.

CERAMICS DIVISION
ARMY MATERIALS AND MECHANICS RESEARCH CENTER
Watertown, Massachusetts 02172

ARMY MATERIALS AND MECHANICS RESEARCH CENTER

MICROSTRUCTURAL AND FRACTOGRAPHIC STUDIES OF BORON CARBIDE SUBJECTED TO BALLISTIC IMPACT AND STATIC FLEXURAL LOADING

ABSTRACT

Microstructural and fractographic studies have been conducted on hot-pressed boron carbide ceramics subjected to ballistic impact by caliber .30 AP M2 projectiles and static flexural loading. A variety of observational techniques were employed, including conventional metallographic and low-power optical examinations, electron microprobe analysis, scanning electron microscopy, and replication electron microscopy. Results suggest that macroscopic topography of fracture-exposed surfaces is indicative of stress states occurring during the fracture event whereas microscopic topography is determined by microstructural constituents, particularly secondary phases, pores, and grain boundaries.

CONTENTS

	Page
ABSTRACT	
INTRODUCTION	1
EXPERIMENTAL	2
RESULTS AND DISCUSSION	
Microstructure and Nonballistic Properties	3
Fracture-Exposed Surfaces	5
SCANNING ELECTRON MICROSCOPY	9
REPLICATION ELECTRON MICROSCOPY	12
CONCLUSIONS	18
ACKNOWLEDGMENTS	20
LITERATURE CITED	21

INTRODUCTION

Ceramic composite armor consisting of a suitable lightweight ceramic adhesively bonded to an extensible fiberglass-reinforced polymeric backup material is presently being employed by the U. S. Army ballistic protection against small arms, armor-piercing (AP) projectiles. From computer studies and complementary ballistic investigations the macroscopic sequence of ballistic interaction and fracture has recently been determined by Wilkins and coworkers for lightweight ceramics impacted by hardened, ogive-shaped small arms projectiles, and desirable material properties for lightweight armor ceramics have been proposed from a continuum viewpoint.[1]

Of all ceramics currently available in sufficiently large sections for lightweight armor application, hot-pressed boron carbide has been demonstrated to display the best ballistic performance.[2] Boron carbide, typically designated B_4C, has a complex crystal structure originally considered to be based on a rhombohedral unit cell having an icosahedron of twelve boron atoms situated at each lattice point and a central linear chain of three carbon atoms. However, it has been found that wide compositional variations in boron carbide are possible without sacrificing essential features of this ideal crystal structure; interchange of boron and carbon atom site occupancy is possible as well as interstitial incorporation of extra atoms in this rather open crystal structure.[3] In practice, boron carbide armor compositions are, moreover, multiphase polycrystalline ceramics with some porosity.

Parallel studies performed by other investigators have provided considerable background information for the present research. Fréchette and Cline, employing a wide range of magnifications, examined fracture-exposed surfaces of a variety of materials, including glass, single-crystal and polycrystalline aluminum oxides, boron carbide, beryllium oxide and steel, following impact by round, flat, and ogive-shaped projectiles.[4] From purely fractographic analyses, the macroscopic fracture sequence resulting from ballistic impact was deduced and found to be in agreement with that predicted from computer studies.[1] It is noteworthy that principal aspects of this macroscopic fracture sequence are qualitatively similar, independent of projectile and impacted material, although microscopic deformation and fracture behavior vary for different materials. Palmour *et al.*[5] investigated fracture-exposed surfaces of single-crystal and polycrystalline aluminum oxides impacted by caliber .30 AP M2 projectiles. From optical microscopy and replication electron microscopy observations, it was found that ballistic fracture of aluminum oxide is frequently characterized by cleavage concluded to be on rhombohedral planes which is particularly extensive in sapphire and probably is responsible* for the inferior ballistic performance[1] of sapphire in comparison to polycrystalline alumina. This observation of preferential ballistic fracture on particular crystallographic planes of aluminum oxide is in general agreement with Wiederhorn's recent measurements of fracture surface energy for cracks propagating on various planes of sapphire.[6] Moreover, preliminary observations by

*Private communication, M. C. F. Cline. Based on experimental results from Light Armor Program conducted at Lawrence Radiation Laboratory and described in Reference 1.

Palmour *et al.* indicated an apparent correlation between ballistic fracture-exposed surface microtopography and fracture sequence, namely that earlier appearing fracture surfaces display greater roughness and are consequently indicative of greater ballistic energy absorption.

The purpose of the present study has been to investigate the mechanical response of hot-pressed boron carbide during ballistic impact from a microstructural viewpoint, i.e., to determine roles of microstructural constituents during ballistic energy absorption and fracture. Ideally, it would be desirable to perform a series of ballistic investigations utilizing well-characterized ceramic specimens in which aspects of a single microstructural variable, such as grain size, porosity, or secondary phase, would be systematically varied over a wide range with other variables held constant. However, ceramic microstructural features are typically interdependent, and such investigations are beyond current ceramic processing technology and would be prohibitively expensive if the technology were available. Alternatively, fractographic studies of boron carbide specimens following ballistic impact by caliber .30 AP M2 projectiles have been performed herein to elucidate both macroscopic and microscopic elements of ballistic fracture. In addition, complementary fractographic studies of four-point bend specimens have been conducted in order to compare fracture-exposed surfaces resulting from ballistic impact with those produced by static loading.

EXPERIMENTAL

Hot-pressed boron carbide of proprietary composition was obtained from Norton Research Corporation (Canada) Ltd., Chippawa, Ontario, Canada, for the present investigation. A single disk approximately 6 inches in diameter and 1/3-inch thick provided specimens for characterization studies, and composite armor specimens formed by adhesively mounting such disks on woven roving tiles approximately 9 inches square and 1/4-inch thick obtained from Russell Reinforced Plastics were ballistically tested utilizing caliber .30 AP M2 projectiles. Further details concerning the procedure[2] for ballistic testing and ballistic performance of these composite armor specimens are available elsewhere.[7]

A variety of characterization studies were performed to establish the microstructural nature and nonballistic properties of this boron carbide. Metallographic specimens were polished and electrolytically etched in HCl.* Preliminary natures of secondary microstructural phases were established by electron beam microprobe analyses.† Density and apparent (open) porosity were determined by a water displacement technique with appropriate corrections for air buoyancy and temperature dependence of water specific gravity. Flexural strength was measured in four-point bending, utilizing a crosshead speed of 0.002"/min. and inner and outer span distances of 1" and 3" on bars 3-1/2" long and 1/4" square. Young's modulus was determined by static means from direct

*Procedure kindly provided in part by Mr. L. J. Beaudin, Norton Research Corporation (Canada) Ltd.; further procedural modifications due to Mr. A. Zeni, AMMRC.

†Conducted at Advanced Metals Research Corporation, Burlington, Massachusetts, under the supervision of Mr. G. Bruno.

strain gage measurements of surface longitudinal strains on tension and compression faces during bend testing and by dynamic means at 10 MHz utilizing the pulse-echo technique.

Fractographic studies were conducted on selected specimens from ballistically impacted disks and fractured bend bars. Optical examinations at low magnifications not exceeding 10X were performed to elucidate elements of macroscopic fracture sequences. Replication electron microscopy provided insight into fracture-exposed surface microtopography, with chromium-shadowed, carbon replicas having an evaporant angle of 27° being employed. In order to bridge these macroscopic and microscopic observations, scanning electron microscopy studies also were performed* as the scanning electron microscope is capable of providing a wide range of magnifications along with an extreme depth of focus. Further discussions of procedures and fractographic applications are available elsewhere for replication electron microscopy[8] and scanning electron microscopy.[9,10]

RESULTS AND DISCUSSION

Microstructure and Nonballistic Properties

The microstructural complexity of the hot-pressed boron carbide obtained for the present study is evident in Figure 1, which contains two micrographs of typical polished surfaces, photographed utilizing polarized light. Besides the boron carbide matrix (phase 1), preliminary electron beam microprobe analyses indicate the presence of at least three additional dissimilar phases whose precise nature is not yet known. Phases 3, 4, and 5 are principally graphitic with apparently some compositional differences. Phase 2, typically appearing as a group of discrete particles, is rich in aluminum, calcium, and silicon, and the whitish-appearing phase 6 is principally composed of titanium. Because their dimensions are considerably smaller than the effective microprobe diameter, preliminary compositional determinations could not be performed for other microstructural phase(s) evident in Figure 1.

Following electrolytic etching with HCl, the microstructural appearance of polished boron carbide is typically that displayed in Figure 2. The matrix grain size is generally of the order of 10μ, but is somewhat nonuniform, ranging in dimensions from under 5μ to about 30μ. Phases appearing in Figure 1 are evident in Figure 2, particularly phase 2 which generally is observed as overetched clusters. A limited amount of twinning, apparent in Figure 2, always was observed in etched microstructures. Comparative microstructural examinations indicated that the incidence of twinning in boron carbide is apparently not enhanced by ballistic impact. A styrofoam-lined box, having an approximately 1-1/2-inch-diameter central hole through which V_{50}-range and low-velocity projectiles were shot, was employed in attempts to capture fragments of the central fracture conoid arising from ballistic impact. However, no conoid fragments suitable for metallographic examination could be obtained from disks impacted by V_{50}-range projectiles, and

*Conducted at Advanced Metals Research Corporation, Burlington, Massachusetts, under the supervision of Mr. G. Bruno.

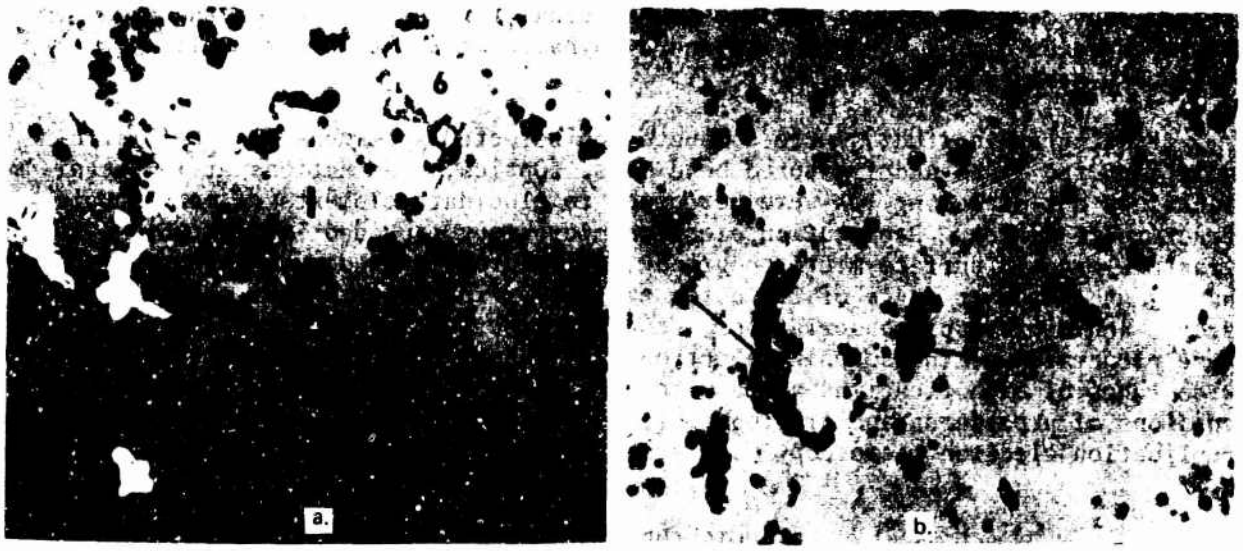

Figure 1. MICROSTRUCTURES OF HOT-PRESSED BORON CARBIDE, PHOTOGRAPHED UTILIZING POLARIZED LIGHT, WITH PRINCIPAL PHASES NUMBERED. SPECIMEN SURFACE POLISHED ONLY. Mag. 1000X

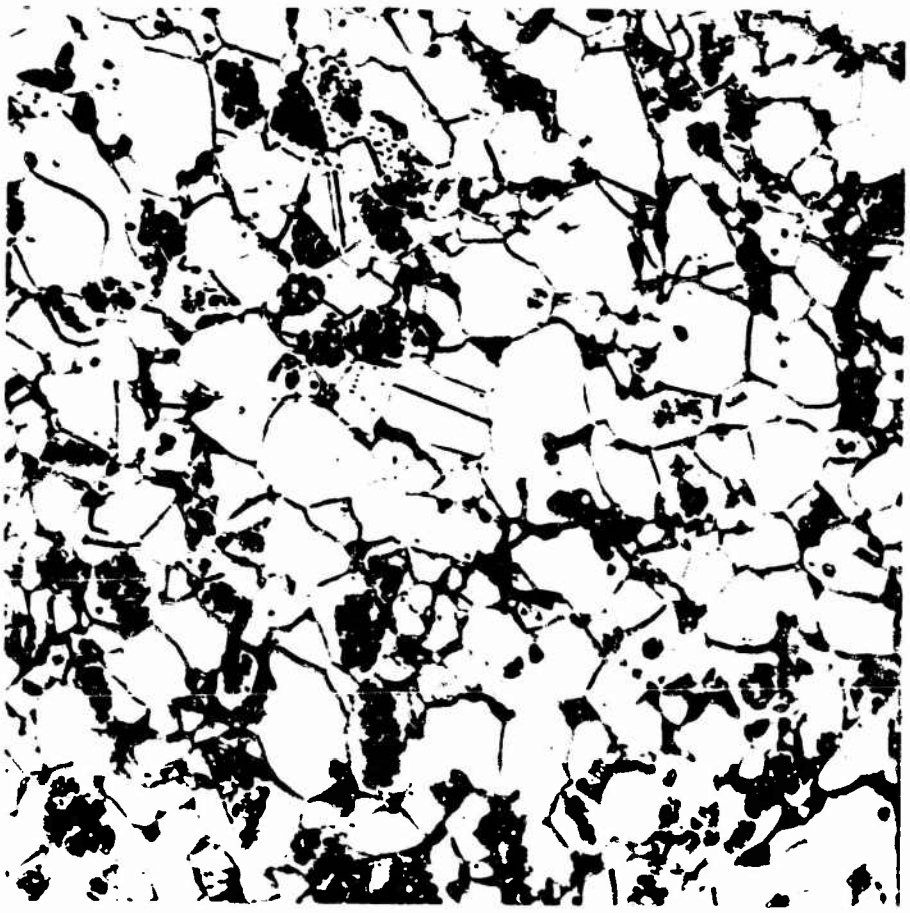

Figure 2. MICROSTRUCTURAL APPEARANCE OF BORON CARBIDE AFTER ELECTROLYTIC ETCHING IN HCl. Mag. 1000X

consequently it was not possible to determine in the present study whether twinning of boron carbide occurs within the conoid as Fréchette and Cline observed for aluminum oxide.[4] It has been suggested* that twinning is a consequence of the hot-pressing procedure employed to fabricate boron carbide, and the incidence of twinning has been found to be highly sensitive to impurities.[7]†

Some nonballistic properties for the boron carbide of the present study are summarized in the table. The reported value for flexural strength is an average for nine specimens; a substantially lower value of 11,500 psi for a tenth specimen has not been included. This abnormally low value and the variation from 41,300 to 55,200 psi for the remaining nine bars are probably due to differing severity of surface flaws introduced during machining test specimens. Part of the difference in values for Young's modulus may be a consequence of slight anisotropy in the hot-pressed disks. The static Young's modulus was measured parallel to the disk face whereas the dynamic Young's modulus was measured orthogonally, parallel to the hot-pressing direction. Apparent or open porosity was very low for this boron carbide. Closed porosity cannot be directly determined by the technique employed here; nevertheless, the total porosity generally was observed to be low (cf. Figure 2).

Nonballistic Properties of Hot-Pressed Boron Carbide	
Flexural strength (four-point bending)	47.8×10^3 psi
Young's modulus	
Static	66.5×10^6 psi
Dynamic	64.7×10^6 psi
Poisson's ratio (dynamic)	0.17
Density	2.51 g/cc
Apparent porosity	<0.1%
Microhardness[7] (Knoop, 100-g load)	2900-3200

Fracture-Exposed Surfaces

Optical Studies

Typical appearances for boron carbide disks of composite armor specimens following impact by caliber .30 AP M2 projectiles are illustrated in Figure 3. The projectile velocity was greater at impact for the specimen illustrated in Figure 3a; moreover, with comparison of projectile remnants it is found that greater erosion has occurred for the projectile of Figure 3a. (This projectile remnant has been sited away from the impact point for convenience of photography.)

The macroscopic appearances of these fracture-exposed surfaces are indicative of both the axially symmetric and dynamic natures of ballistic loading. From examination of these macrophotographs many features of the ballistic

*Private communication, Messrs. B. Matchen and L. Beaudin, Norton Research Corporation (Canada) Ltd.
†Private communication, Mr. G. Q. Weaver, Norton Company, Worcester, Massachusetts.

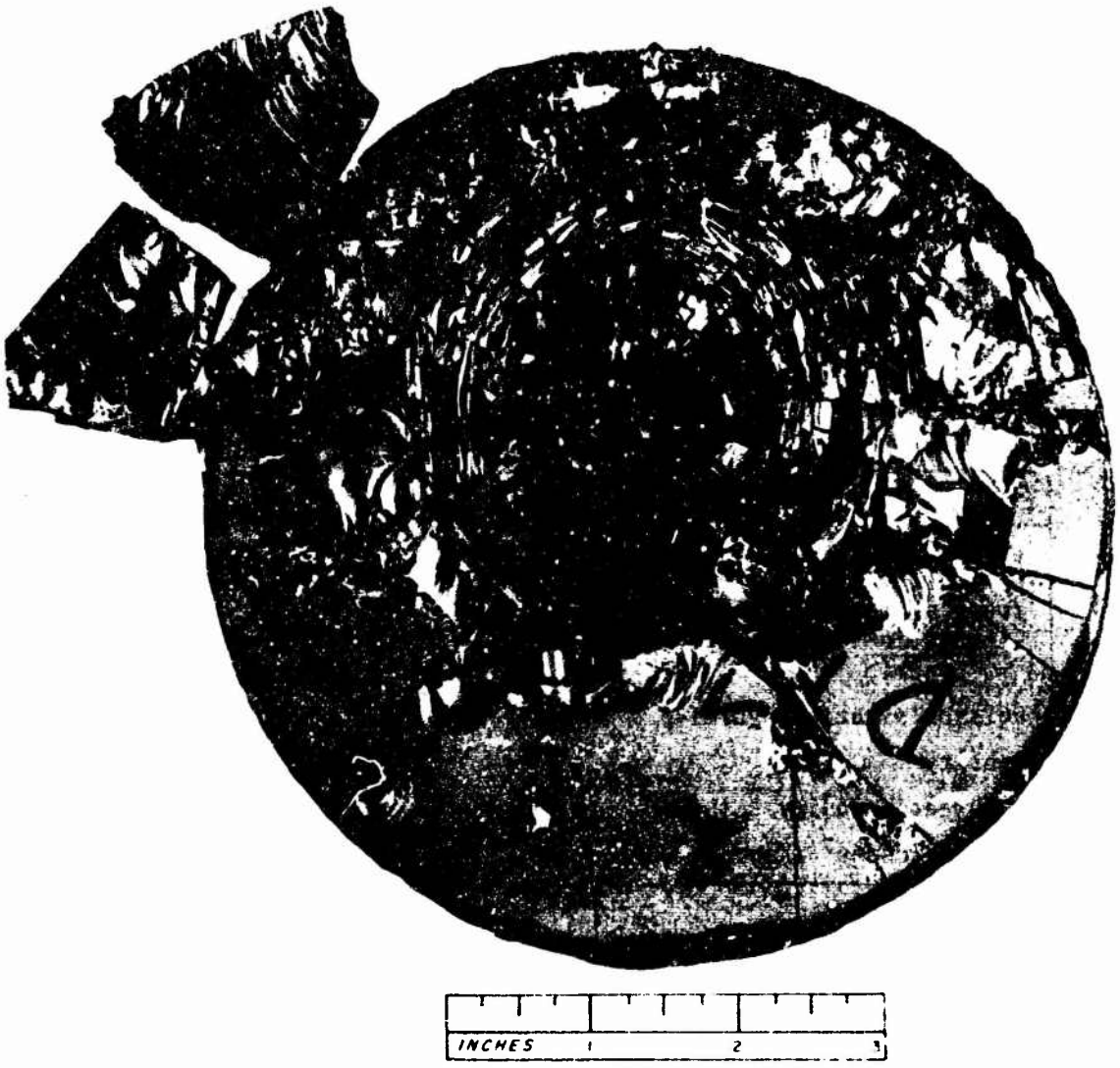

a. Overall Appearance

Figure 3. MACROSCOPIC FRACTURE-EXPOSED SURFACES FOR BORON CARBIDE DISKS OF COMPOSITE ARMOR SPECIMENS FOLLOWING IMPACT BY CALIBER .30 AP M2 PROJECTILES

19-066-272/AMC-70

b. Appearance for Lower Impacting Projectile Velocity. Mag. 2X

Figure 3. MACROSCOPIC FRACTURE-EXPOSED SURFACES FOR BORON CARBIDE DISKS OF COMPOSITE ARMOR SPECIMENS FOLLOWING IMPACT BY CALIBER .30 AP M2 PROJECTILES

19-066-265/AMC-70

fracture sequence can be deduced; this fracture sequence and prominent topographical characteristics are similar to those reported by Fréchette and Cline[4] and by Long and Brantley* for a variety of ceramics. Comminuted fragments therefrom were too minute for reconstruction of fracture conoids and efforts to preserve intact significant portions of conoids by utilizing low-velocity projectiles were unsuccessful. Hence, the initial sequence within the fracture conoid could not be determined in the present study although details are reported elsewhere.[4]

After the fracture conoid, major radial cracks having included angles of about 30° are the first elements of the fracture patterns in Figure 3 to form. This result follows from the discontinuity in fracture-exposed surface topography across each major radial crack. Within each resulting sector bounded by two major radial cracks, the fracture-exposed surface lying approximately parallel to the tile face is observed in Figure 3 to have a corrugated appearance, particularly from the vicinity of the impact axis to about halfway toward the tile periphery. It is plausible that within each sector a fracture front sweeps radially outward, initiated near the impact axis (at or within the initial fracture conoid); the corrugated topography is attributed to modulation of the axial tensile stress by radial and circumferential tensile stresses, with the corrugation wavelength indicative of stress wave reverberation. In fact, within each major sector there are a number of approximately parallel such fracture surfaces having corrugated appearances, particularly near the impact axis. It should be possible to relate the distance between these fracture surfaces to the axial impact stress and the dynamic tensile strength of boron carbide.

Secondary radial cracks having included angles of about 10° are also prominent within each major fracture section. Because of the continuity of corrugated surface topography across secondary radial cracks, these latter features occur after the corrugated surfaces are formed; it is presumed that the secondary radial cracks also are initiated near the impact axis. Less prominent in Figure 3 are circumferential cracks which occur subsequent to major radial cracks but typically precede secondary radial cracks. Late-time, spall-like fractures frequently are observed toward the periphery of the front face; a number of these features are apparent in Figure 3a, the fractures having been initiated at various points along radial cracks separating the large fragments most remote from the impact site. Other late-time fractures are conspicuous at the northwest quadrant of Figure 3a (where mating fragments have been placed outside corresponding major sectors) and near the bottom of Figure 3b. The curved topographical features are concave in the direction of the initiation point for each region of fracture.

In contrast, there is considerable difference in macroscopic appearance for fracture-exposed surfaces of flexural test bars in comparison to ballistic specimens, indicative of the dissimilar stress states occurring during these two fracture events. A fragment from a fractured bend bar is illustrated in Figure 4; portion of a wire and other remnants from a strain gage assembly are visible at the right side of this fragment. During mechanical testing the original bar

*LONG, W. D. and BRANTLEY, W. A. *Fractographic Analyses of Densified Ceramics and Glass-Ceramics Ballistically Impacted by Caliber .30 M2 Projectiles.* Army Materials and Mechanics Research Center, AMMRC TR 70-17, July 1970.

fractured into three principal fragments, yielding another fragment similar in appearance to the one illustrated and a smaller fragment which originally was situated between the larger fragments prior to fracture. Upon examination of these three fragments, it was found that following initiation two separate major fracture fronts propagated in approximately symmetric senses on opposite sides of a vertical plane (i.e., normal to the neutral axis) through the initiation region, ultimately yielding the principal fragments.

Figure 4. MACROSCOPIC FRACTURE-EXPOSED SURFACE OF BORON CARBIDE BAR FOLLOWING FAILURE IN FOUR-POINT BENDING. Mag. 10X

For the fragment depicted in Figure 4, fracture was initiated at the lower left corner, near the surface of the face under tensile stress during flexural loading. A major fracture front then swept radially outward, generating subsequently the two prominent furrows which diverge away from the initiation region. Surface topographical features indicate local reorientation of principal stress axes occurring during passage of the crack front.[11] Over the central portion of the fracture-exposed surface, fracture propagation was normal to the curved topographical features, as indicated by a number of parallel linear features. The termination region is characterized by turning of the fracture propagation path in order to intersect the surface orthogonally.

SCANNING ELECTRON MICROSCOPY

Representative regions from fragments illustrated in Figures 3a and 4 have been studied at magnifications ranging from 24X to 6000X, utilizing the scanning electron microscope, to provide insight into relationships between macroscopic and microscopic fracture behavior. In discussions thus far, it has been concluded that macroscopic fracture-exposed surface topography is principally determined by local stress states existing during the fracture event. Observations at higher magnifications suggest that the fine structure of fracture-exposed surface topography is principally dependent on microstructural constituents for the boron carbide employed in the present study.

Two specimens were selected for examination from the fractured ballistic specimen of Figure 3a: a slender wedge-shaped fragment (A) lying within less

than 1 inch of the impact axis and situated at the rear of the ceramic; a truncated, wedge-shaped fragment (B) located about 1-1/2 inches from the impact axis and prominently displaying the previously discussed corrugated fracture surface. A region from the face of fragment A located parallel to and nearest the impact axis is illustrated at two magnifications in Figure 5. The extremely great roughness of surface topography is evident and indicative presumably of substantial conversion from ballistic impact energy to fracture surface energy. Further study of this particular fracture behavior is necessary; the scale of topographical features is apparently less than the average grain size (cf. Figure 2). Various regions from the top surface of fragment A are illustrated in Figure 6. The predominant fracture mode is apparently intergranular, and considerable debris* of unknown composition, ranging in dimensions from approximately 0.2 to 10μ, are generated during fracture. Moreover, it is evident that secondary phases and porosity significantly affect fracture propagation as regions of fracture are induced to intersect these defects; the faceted pore at the grain boundary of Figure 6b and the cluster of pores and secondary phase pull-outs in Figure 6c are of particular interest. Although the angular appearance of the defects may suggest pull-outs rather than pores, unambiguous interpretation of such features is difficult.

A region from the corrugated top surface of fragment B is illustrated in Figure 7 at three successively greater magnifications. Corrugated topographical features lying in approximately a vertical direction are visible in Figure 7a, along with parallel horizontal features lying along the path of fracture propagation. At higher magnifications, it is found that the fracture mode still is predominantly intergranular though some evidence of transgranular fracture is observed. Additional support for the strong influence of porosity and secondary phases on fracture behavior is available from Figures 7b and 7c as fracture

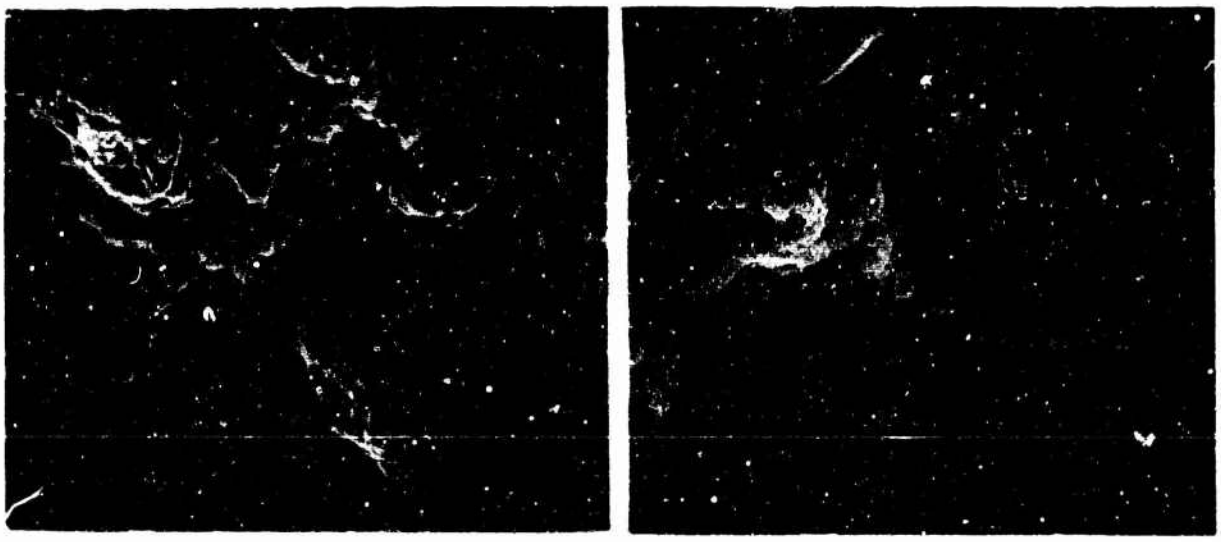

Figure 5. REGION OF FACE PARALLEL TO AND NEAREST IMPACT AXIS FROM FRAGMENT LOCATED ORIGINALLY AT REAR CENTER OF BALLISTIC TILE ILLUSTRATED IN FIGURE 3a.

a. Mag. 320X b. Mag. 1600X

*Specimen surfaces providing Figures 7 through 11 were cleaned ultrasonically prior to examination in order to remove such debris which tends to obscure underlying surface details (cf. Figure 6d).

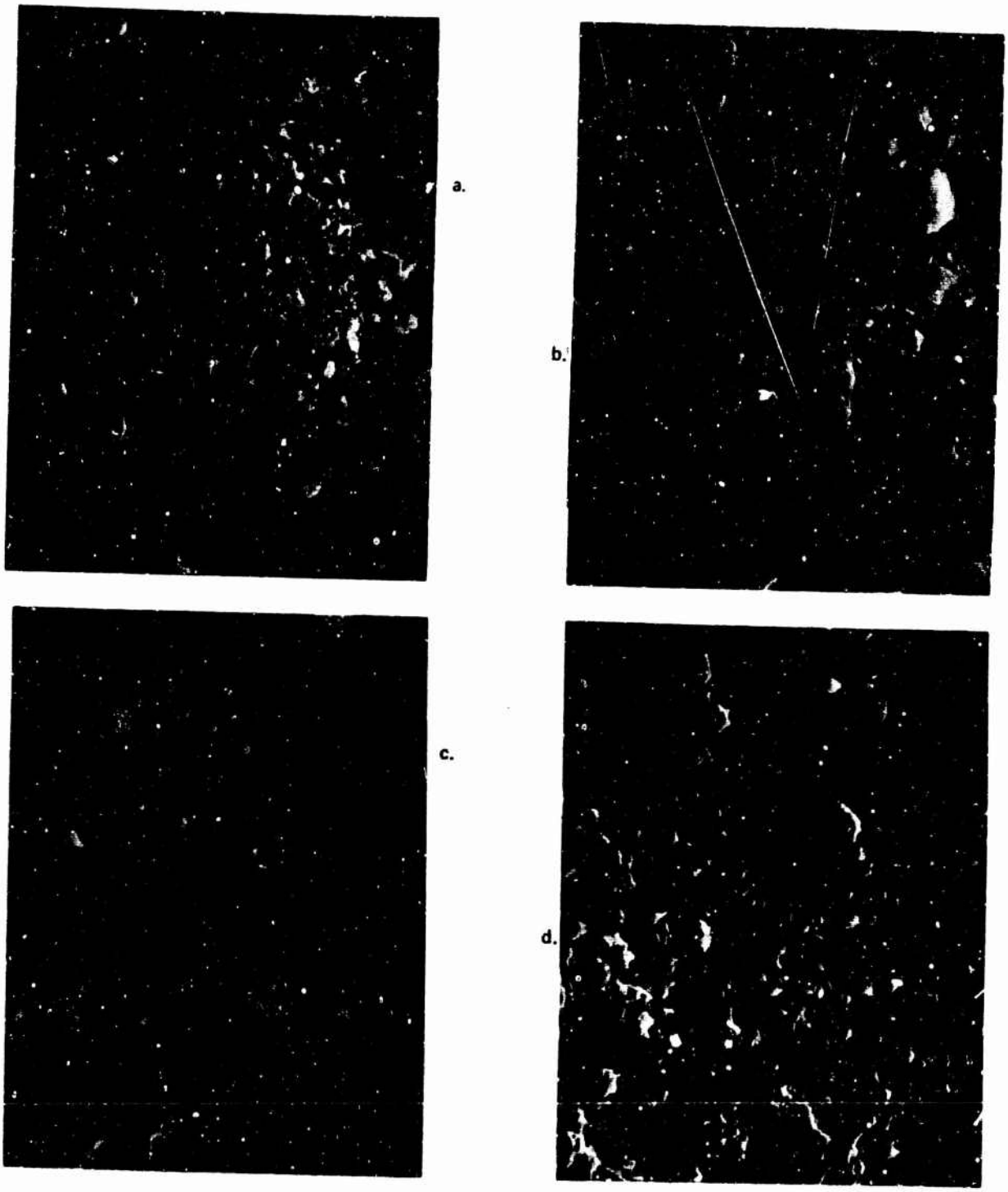

Figure 6. REGIONS FROM TOP SURFACE OF FRAGMENT WHOSE END SURFACE IS ILLUSTRATED IN FIGURE 5.

a. First Region. Mag. 500X
b. First Region. Mag. 2000X
c. Second Region. Mag. 2000X
d. Third Region. Mag. 600X

fronts again often are induced to intersect these defects. A region from the lateral surface of fragment B, representative of radial fracture-exposed surfaces, is illustrated in Figure 8. Although present results are preliminary, the roughness of topographical features appears greater here than for Figure 7. Again fracture is generally intergranular, but some indications, presumably river patterns, of transgranular fracture are visible in Figure 8b.

For comparison, areas from the fracture propagation and termination regions of the smaller fragment mating the one illustrated in Figure 4 are shown in Figures 9, 10, and 11. The difference in fracture characteristics of the three areas is noteworthy. Fracture within that portion of the propagation region near the prominent furrows of Figure 4 is both intergranular and transgranular in Figure 9, with prominent river patterns evident for the latter fracture mode. Within later portions of the propagation region (Figure 10) predominantly intergranular fracture is observed, and fracture-exposed surfaces display relatively smooth topography. However, a duplex surface topography appears to arise within the termination region, for areas of considerable fine-scale roughness (cf. Figure 5) are adjacent to smoother areas of intergranular fracture; further study is necessary to characterize this fracture behavior. It is also evident from numerous examples in Figures 9, 10, and 11 that porosity and secondary phases strongly influence fracture propagation during static flexural fracture.

REPLICATION ELECTRON MICROSCOPY

Replicas of ballistic fracture-exposed surfaces comprise Figures 12 through 15, wherein areas were selected from top corrugated surfaces of three wedge-shaped fragments lying at various distances from the impact axis. Different areas from the same fragment which lay farthest from the impact axis are illustrated in Figures 12 and 13 whereas the fragment providing Figure 15 was nearest the impact axis. (No replicas were made from radial fracture-exposed surfaces or surfaces similar to that displayed in Figure 5; studies of such replicas are suggested for future work.) In all four illustrations, river patterns characteristic of transgranular fracture are evident. The local fracture propagation direction is parallel to the river patterns in the direction of converging tributaries for a given river marking.[8,11] Thus, the fracture direction in Figure 13 was from northeast to southwest; particularly noteworthy are crack interactions with several pores and a grain boundary. (Alternatively, these shallow features may result from fracture around minute spherical secondary phase particles similar to those apparent in Figure 15.) In Figure 15 the transgranular fracture swept approximately from south to north, the fracture mode altering at the grain boundary to intergranular. (Horizontal white streaks and dark regions near the top of Figure 15 are artifacts of replication as river markings and other features are clearly visible through these streaks and dark regions.) In Figure 12, several different local fracture propagation directions are evident, indicating a more complex sequence of fracture; moreover, the crack front apparently was induced to intersect the cluster of defects prominent in the upper left of this illustration. Some intergranular fracture appeared to occur at relatively steep grain boundaries near the center and bottom of Figure 12, but insufficient topographical resolution prevented further analysis. Preliminary transmission electron microscopy studies were conducted on a large, thin flake captured in the replicating tape but no contrast effects attributable to dislocations were

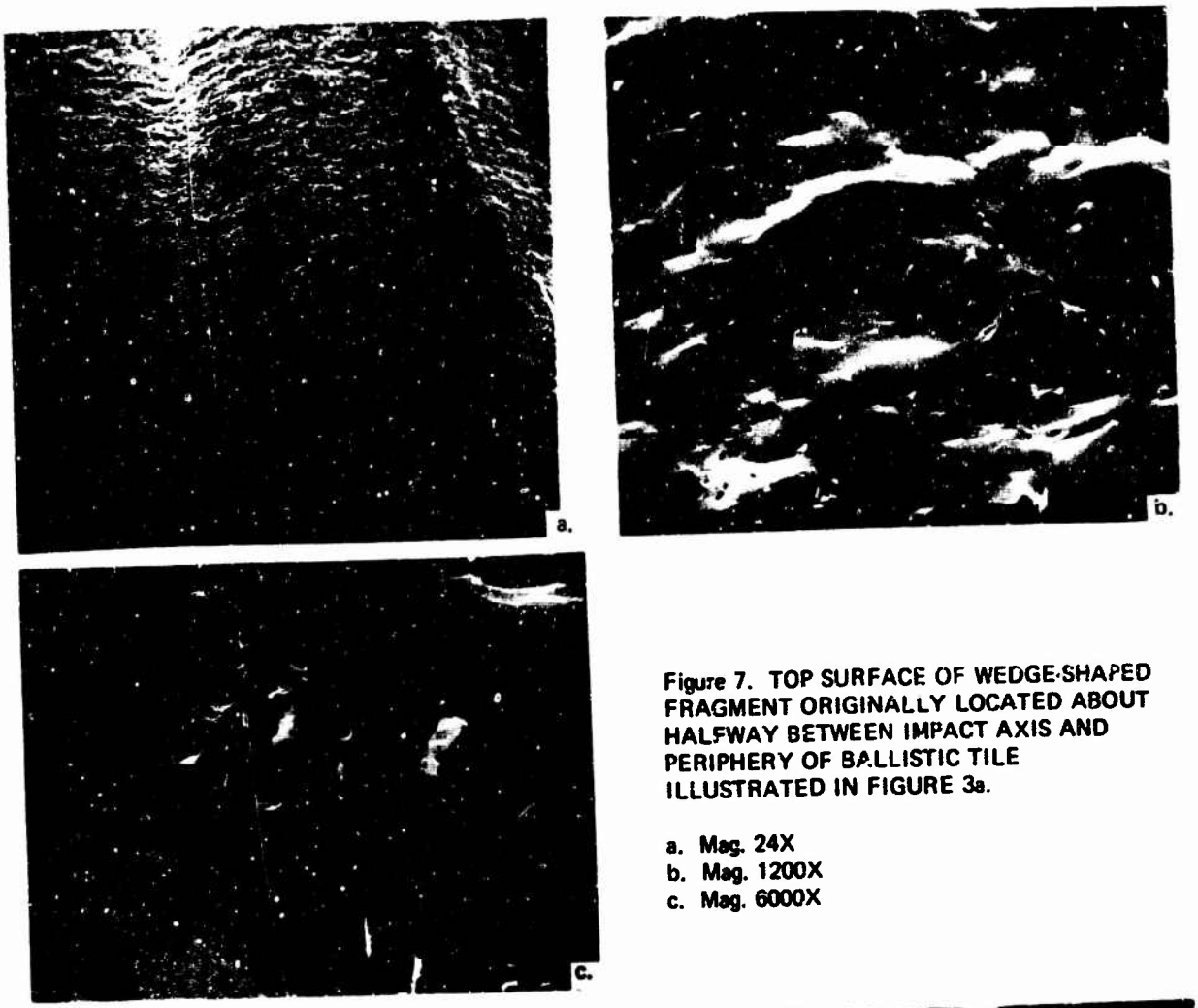

Figure 7. TOP SURFACE OF WEDGE-SHAPED FRAGMENT ORIGINALLY LOCATED ABOUT HALFWAY BETWEEN IMPACT AXIS AND PERIPHERY OF BALLISTIC TILE ILLUSTRATED IN FIGURE 3a.

a. Mag. 24X
b. Mag. 1200X
c. Mag. 6000X

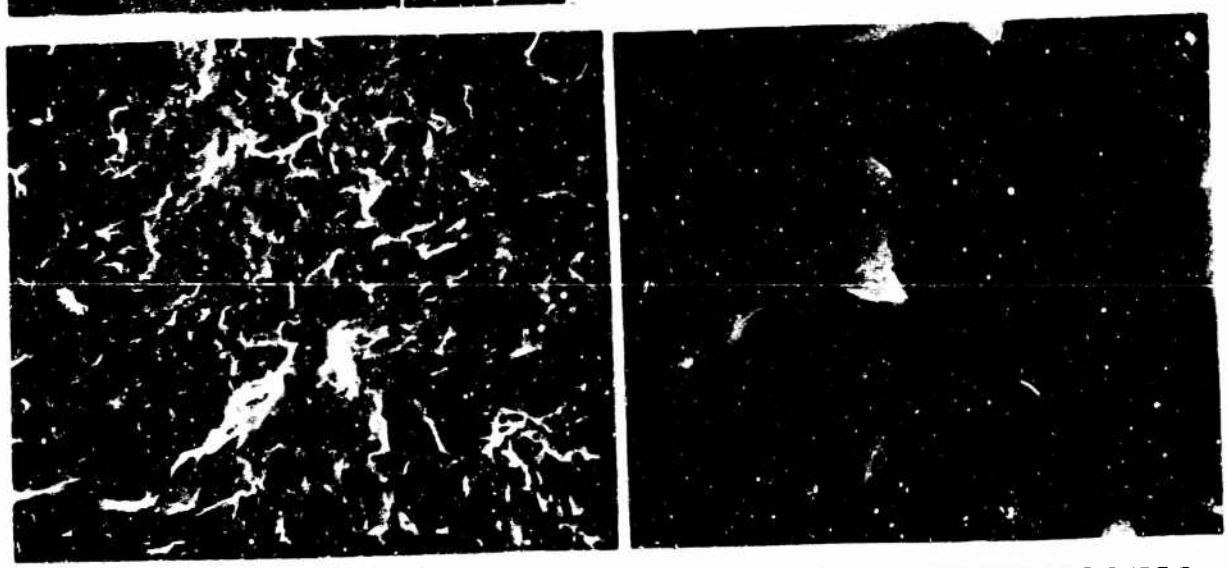

Figure 8. LATERAL SURFACE OF FRAGMENT WHOSE TOP SURFACE IS ILLUSTRATED IN FIGURE 5
a. Mag. 300X b. Mag. 3000X

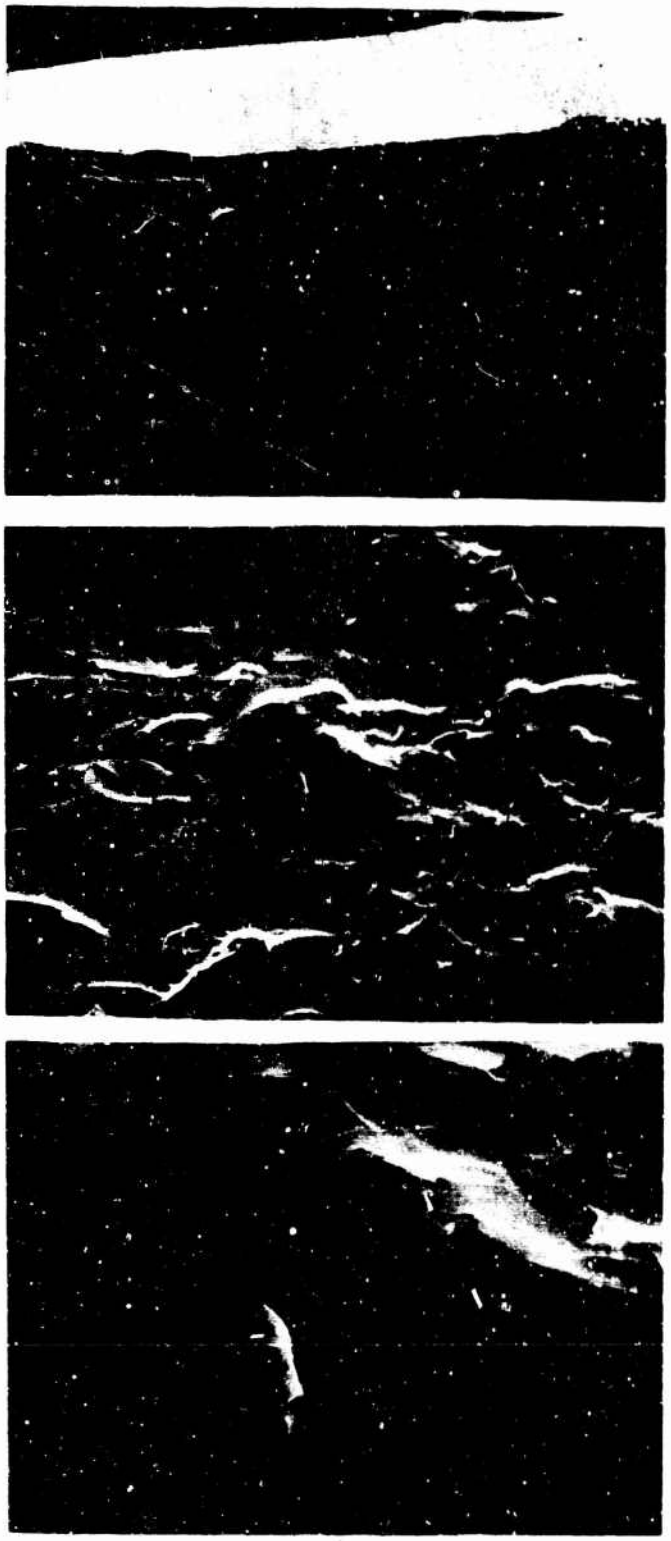

a. Mag. 26X

b. Mag. 650X

c. Mag. 2600X

Figure 9. FRACTURE PROPAGATION REGION OF BEND BAR FRAGMENT ORIGINALLY MATING THE FRAGMENT ILLUSTRATED IN FIGURE 4

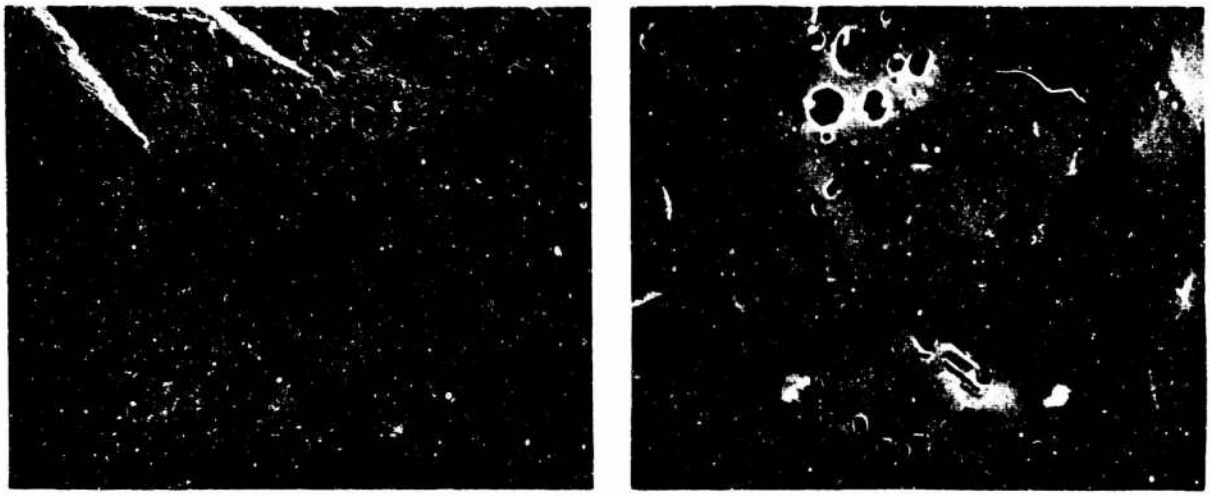

a. Mag. 24X b. Mag. 2400X

Figure 10. LATER FRACTURE PROPAGATION REGION FOR THE BEND BAR FRAGMENT ILLUSTRATED IN FIGURE 9

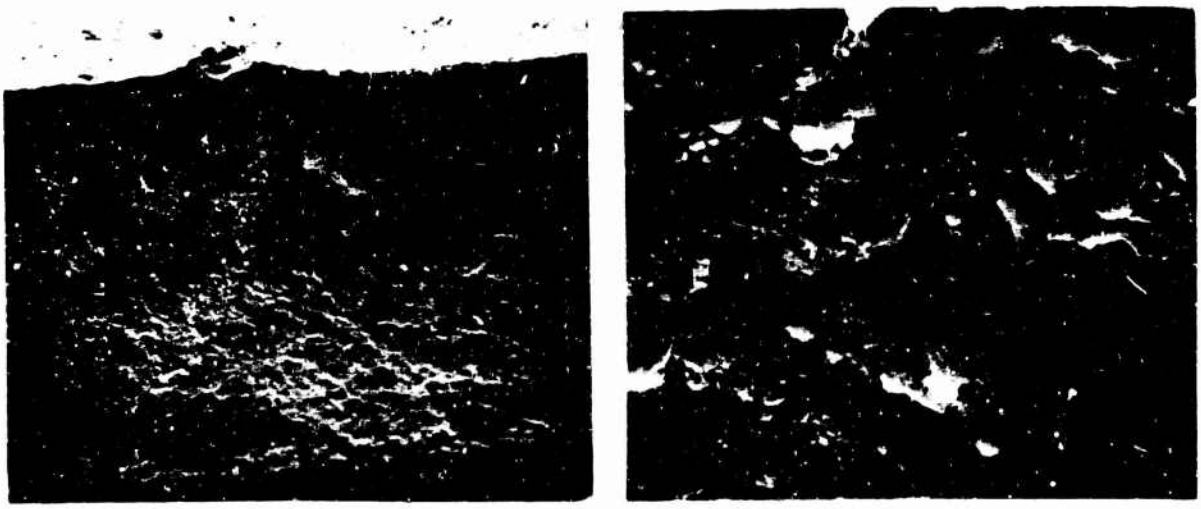

a. Mag. 65X b. Mag. 1300X

Figure 11. FRACTURE TERMINATION REGION FOR BEND BAR FRAGMENT ILLUSTRATED IN FIGURES 9 AND 10

Figure 12. AREA FROM TOP SURFACE OF LARGE WEDGE-SHAPED FRAGMENT LOCATED NEAR PERIPHERY OF BALLISTIC TILE. Mag. 10900X

Figure 13. DIFFERENT AREA FROM SAME TOP SURFACE OF FRAGMENT SHOWN IN FIGURE 12. Mag. 7900X

Figure 14. AREA FROM TOP SURFACE OF FRAGMENT LOCATED ABOUT MIDWAY BETWEEN IMPACT AXIS AND PERIPHERY OF BALLISTIC TILE. DEBRIS GENERATED DURING FRACTURE AND CAPTURED DURING REPLICATION IS PARTICULARLY CONSPICUOUS. Mag. 17500X

Figure 15. AREA FROM TOP SURFACE OF FRAGMENT LOCATED NEAR IMPACT AXIS. Mag. 15000X

observed. Consequently, the nature of this flake, seen in the lower left portion of Figure 14, was not determined by electron diffraction although it is presumed to be boron carbide.

As is the case for ballistic fracture-exposed surfaces, replicas from areas of the bend bar fragment illustrated in Figure 4 display minute topographical details somewhat at the sacrifice of depth of resolution. Areas from the fracture propagation and termination regions are illustrated in Figures 16 and 17 and present appearances rather similar to those in Figures 6 through 15. A great amount of minute transgranular fracture details are evident everywhere in Figure 16, with some examples of intergranular parting resulting in generally flat, featureless topography. Although the general direction for much of the fracture in this illustration is approximately from left to right, many examples of crack propagation in other directions are apparent. Little additional insight into fracture characterization for the termination region is possible from Figure 17 because topographical details cannot be resolved (cf. Figure 11b); the parallel features running from northeast to southwest are presumably parallel to the path of fracture propagation.

Although some transgranular fracture of boron carbide occurs during ballistic impact and flexural loading, there are apparently no preferential fracture planes giving rise to cleavage in the manner observed by Palmour *et al.*[5] for aluminum oxide. At the present time, it is uncertain whether the observed fracture behavior is intrinsic to boron carbide or the result instead of impure boron carbide with porosity and possibly local variations in B:C stoichiometry; it is plausible, considering the cleavage occurring for other covalent crystals, that the latter case is likely.

CONCLUSIONS

The hot-pressed boron carbide utilized in the present investigation has a complex, multiphase microstructure with some porosity. In addition to the boron carbide matrix, electron microprobe analyses indicate the presence of at least three additional secondary phases. Other phases having particulate dimensions less than the effective microprobe diameter also may be present. Although twinning of the boron carbide matrix sometimes is observed, the incidence of twinning apparently is not significantly increased by ballistic impact. However further study of fragments from ballistic fracture conoids is necessary before this preliminary conclusion is definite.

Low-power optical observations suggest that macroscopic fracture-exposed surface topography is indicative of stress states occurring during the fracture event for both ballistic impact and flexural loading. From scanning electron microscopy and replication electron microscopy observations it is found that microscopic fracture behavior is determined by microstructural constituents. Although both transgranular and intergranular fracture modes are observed, intergranular fracture apparently is predominant. Moreover, fracture fronts typically are strongly influenced by secondary phases and pores. There are apparently no preferential fracture planes for boron carbide as cleavage is not observed, but at present insufficient evidence is available to consider this fracture behavior intrinsic to boron carbide.

Figure 16. PROFUSE DETAIL OF SURFACE FROM FRACTURE PROPAGATION REGION OF FRAGMENT ILLUSTRATED IN FIGURE 4. Mag. 8500X

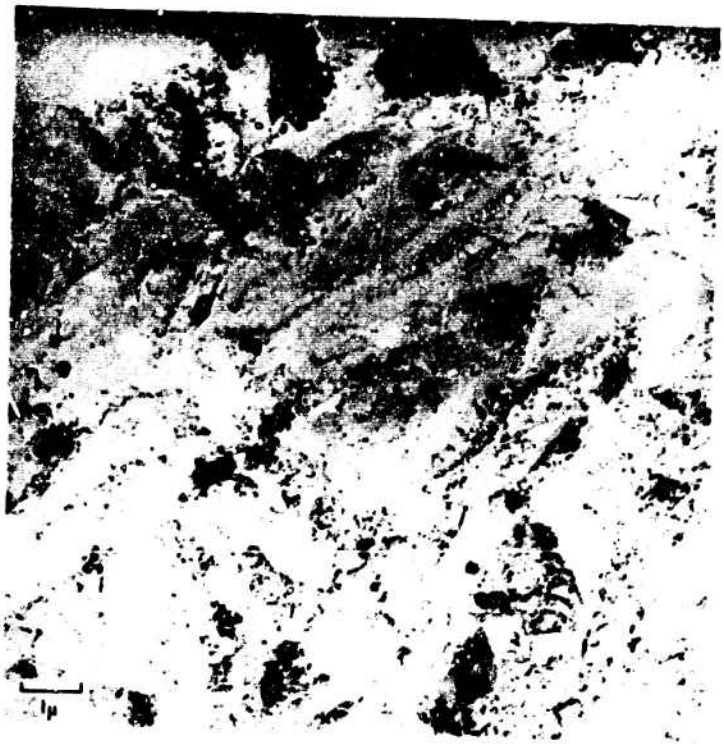

Figure 17. DUPLEX CHARACTER OF SURFACE FROM FRACTURE TERMINATION REGION OF FRAGMENT ILLUSTRATED IN FIGURE 4. Mag. 8500X

ACKNOWLEDGMENTS

It is a pleasure to acknowledge contributions from a large number of individuals during this investigation. Particular thanks are extended to Messrs. B. Matchen and L. Beaudin of Norton Research Corporation (Canada) Ltd. for many helpful comments concerning hot-pressed boron carbide and to Professor V. D. Fréchette who kindly provided a copy of his presentation cited in Reference 4. Electron microprobe analyses and scanning electron microscopy observations were conducted at Advanced Metals Research Corporation, Burlington, Massachusetts, under the supervision of Mr. G. Bruno. Preparation of replicas and considerable assistance with electron microscopy observations were provided by Mr. M. Dumais, formerly of AMMRC. Individuals from AMMRC gratefully thanked for important contributions are Messrs. H. O'Connell and S. Acquaviva for conducting the flexural strength testing and strain gage measurements; Messrs. A. Zani, F. Cotter, W. Duffy, and S. Nanfria for metallographic and photographic services; Messrs. C. Polley, A. DiCologero, S. Favuzza, and H. Jodoin for performing the ballistic investigation; Mr. R. Brockelman for ultrasonic wave speed measurements; and Mr. P. Norman for measurements of density and apparent porosity. Finally, stimulating discussions regarding interpretations of scanning electron micrographs were held with Dr. R. Katz of AMMRC who kindly showed results from his independent fractographic studies of boron carbides. His assistance and that of Mr. S. Acquaviva in reviewing this report are gratefully appreciated.

LITERATURE CITED

1. WILKINS, M. L., CLINE, C. F., and HONODEL, C. A. *Fourth Progress Report of Light Armor Program.* Lawrence Radiation Laboratory. Livermore, California, Report No. UCRL 50694, June 1969.

2. MASCIANICA, F. S. *Summary of Terminal Ballistic Data on Lightweight Armor Materials (U).* (Confidential Report), Army Materials and Mechanics Research Center, Watertown, Massachusetts, AMMRC TR 69-17, July 1969.

3. HOARD, J. L., and HUGHES, R. E. *Elemental Boron and Compounds of High Boron Content: Structure, Properties, and Polymorphism.* The Chemistry of Boron and its Compounds, Earl Muetterties ed., John Wiley and Sons, Inc., New York, 1967, p. 38-73.

4. FRÉCHETTE, V. D., and CLINE, C. F. *Fractography of Ballistically Tested Ceramics.* Presented at the 71st Annual Meeting of the American Ceramic Society, Washington, D. C., May 1969.

5. PALMOUR, III, H., KIM, C. H., JOHNSON, D. R., and ZIMMER, C. E. *Fractographic and Thermal Analyses of Shocked Alumina.* North Carolina State University, Office of Naval Research Contract N00014-68-A-0187; NR 064-504, Technical Report 69-5, April 1969.

6. WIEDERHORN, S. *Fracture of Sapphire.* Journal of the American Ceramic Society, v. 52, no. 9, September 1969, p. 485-491.

7. MATCHEN, B. *Joint U.S.-Canadian Defense Development Sharing Project on Ceramic Armour Materials (U).* (Confidential Report), Norton Research Corporation (Canada) Ltd. Contract No. DAAG46-68-C-0096 (U.S.) and Contract No. 91-522; Serial No. 4 ME-16 (Canadian), Interim Technical Report, 1 December 1967 to 24 May 1969, and Final Report, in process.

8. PHILLIPS, A., KERLINC, V., and WHITESON, B. V. *Electron Fractography Handbook.* Douglas Aircraft Company, Inc., Contract No. AF 33 (657) - 11127, Air Force Materials Laboratory, Wright-Patterson Air Force Base, Technical Report ML-TDR-64-416, January 1965. (AD 612912)

9. JOHARI, O. *Comparison of Transmission Electron Microscopy and Scanning Electron Microscopy of Fracture Surfaces.* Journal of Metals, v. 20, no. 6, June 1968, p. 26-32.

10. JOHARI, O., and PARIKH, N. M. *Fracture Mechanisms in Polycrystalline Nonmetallic Materials.* IIT Research Institute, Contract DAAG46-67-C-017, AMMRC Final Technical Report, CR 69-02(F), April 1968.

11. FRÉCHETTE, V. D. *Characteristics of Fracture-Exposed Surfaces.* Proceedings of the British Ceramic Society, no. 5, December 1966, p. 97-106.

UNCLASSIFIED
Security Classification

DOCUMENT CONTROL DATA - R & D

(Security classification of title, body of abstract and indexing annotation must be entered when the overall report is classified)

1. ORIGINATING ACTIVITY *(Corporate author)* Army Materials and Mechanics Research Center Watertown, Massachusetts 02172	2a. REPORT SECURITY CLASSIFICATION Unclassified 2b. GROUP

3. REPORT TITLE

MICROSTRUCTURAL AND FRACTOGRAPHIC STUDIES OF BORON CARBIDE SUBJECTED TO BALLISTIC IMPACT AND STATIC FLEXURAL LOADING

4. DESCRIPTIVE NOTES *(Type of report and inclusive dates)*

5. AUTHOR(S) *(First name, middle initial, last name)*

William A. Brantley

6. REPORT DATE August 1970	7a. TOTAL NO. OF PAGES 24	7b. NO. OF REFS 11
8a. CONTRACT OR GRANT NO. b. PROJECT NO. D/A 1T062105A330 c. AMCMS Code 502E.11.296 d. Agency Accession Number DA OB4802	9a. ORIGINATOR'S REPORT NUMBER(S) AMMRC TR 70-18 9b. OTHER REPORT NO(S) *(Any other numbers that may be assigned this report)*	

10. DISTRIBUTION STATEMENT

This document has been approved for public release and sale; its distribution is unlimited.

11. SUPPLEMENTARY NOTES	12. SPONSORING MILITARY ACTIVITY U. S. Army Materiel Command Washington, D. C. 20315

13. ABSTRACT

Microstructural and fractographic studies ~~have been~~ conducted on hot-pressed boron carbide ceramics subjected to ballistic impact by caliber .30 AP M2 projectiles and static flexural loading. A variety of observational techniques were employed, including conventional metallographic and low-power optical examinations, electron microprobe analysis, scanning electron microscopy, and replication electron microscopy. Results suggest that macroscopic topography of fracture-exposed surfaces is indicative of stress states occurring during the fracture event whereas microscopic topography is determined by microstructural constituents, particularly secondary phases, pores, and grain boundaries. (Author)

DD FORM 1 NOV 65 1473 REPLACES DD FORM 1473, 1 JAN 64, WHICH IS OBSOLETE FOR ARMY USE.

UNCLASSIFIED
Security Classification

UNCLASSIFIED

Security Classification

14 KEY WORDS	LINK A ROLE	LINK A WT	LINK B ROLE	LINK B WT	LINK C ROLE	LINK C WT
Fractography						
Terminal ballistics						
Mechanical properties						
Lightweight armor						
Ceramics						
Boron carbide						
Microstructure, ceramic						

UNCLASSIFIED

Security Classification